Monomorphous decomposition method and its application for phase retrieval and phase-contrast tomography

T. E. Gureyev,[1,2,3,4] Ya. I. Nesterets,[4,2] and D. M. Paganin[3]

[1]*ARC Centre of Excellence in Advanced Molecular Imaging, School of Physics, The University of Melbourne, Parkville VIC 3010, Australia*
[2]*School of Science and Technology, University of New England, Armidale NSW 2351, Australia*
[3]*School of Physics and Astronomy, Monash University, Clayton VIC 3800, Australia*
[4]*Commonwealth Scientific and Industrial Research Organisation, Clayton VIC 3168, Australia*

(Received 27 July 2015; published 30 November 2015)

We show that an arbitrary spatial distribution of complex refractive index decrement inside an object can be exactly represented as a sum of two "monomorphous" complex distributions, i.e., distributions with the ratios of the real part to the imaginary part being constant throughout the object. *A priori* knowledge of constituent materials can be used to estimate the global lower and upper boundaries for this ratio. This "monomorphous decomposition" approach can be viewed as an extension of the successful phase-retrieval method, based on the transport of intensity equation, that was previously developed for monomorphous (homogeneous) objects, such as, e.g., objects consisting of a single material. We demonstrate that the monomorphous decomposition can lead to more stable methods for phase retrieval using the transport of intensity equation. Such methods may find application in quantitative in-line phase-contrast imaging and phase-contrast tomography.

DOI: 10.1103/PhysRevA.92.053860 PACS number(s): 42.30.Rx, 42.30.Wb, 87.59.−e

I. INTRODUCTION

The use of the transport of intensity equation (TIE) [1,2] for solving the problem of optical phase retrieval, i.e., the problem of reconstruction of the phase distribution of the complex amplitude of a free-propagating optical beam from one or more measurements of its intensity distribution in the plane(s) orthogonal to the optic axis in the Fresnel region, has been extensively investigated since the publication of a seminal paper by Teague [2] in 1983. The approach was successfully applied in infrared adaptive optics [3] and electron microscopy [4,5], and later in x-ray imaging [6–23], visible light microscopy [24,25], and elsewhere. The success of the method led to a large number of studies which reported various implementations of the TIE-based phase retrieval and the validity limits for the method. In particular, it has been shown [12] that in order to achieve quantitatively accurate phase retrieval, the propagation-induced contrast (i.e., the difference between the image distributions in the object and image planes) must be weak. This condition typically leads to low signal-to-noise ratios and, consequently, to poor numerical stability in the associated phase retrieval which affects primarily the low-spatial-frequency components of the reconstructed phase distributions. Here we propose a method that can potentially alleviate this instability with the help of generic *a priori* information about the sample.

As a motivation for the key idea underpinning the present work, we note the oft-made comment that, for the purposes of x-ray imaging simulation, human tissues can be well approximated by a superposition of aluminum and water. This striking statement is paralleled by the fact that many tissue-mimicking phantoms, for several forms of medical imaging, are composed of a small number of particular materials [26]. As will be shown in the present paper, the "aluminum and water" approximation is not as crude as it initially sounds. Specifically, as a key enabling result for the present paper, we show that an arbitrary three-dimensional distribution of complex refractive index can be *exactly* represented at any particular x-ray energy (wavelength) as a sum of two interpenetrating "monomorphous" complex distributions, i.e., two distributions for each of which the ratios of the real part to the imaginary part of the complex refractive index decrement are constant throughout the object. This implies, for example, that for x-ray scattering purposes the human body can be *exactly* represented by a three-dimensional distribution of aluminum interpenetrating a three-dimensional distribution of water. Moreover, to within the degree of approximation that the body can be represented by a complex refractive index, this decomposition is exact and applicable to all forms of scattering of probe radiation incident upon a sample which can be well described with a complex refractive index or potential.

The above "monomorphous decomposition" approach constitutes a practical simplification of the forward problem [22] of determining the scattered intensity distribution due to paraxial (i.e., beamlike) complex monochromatic scalar fields scattering from a slowly-spatially-varying distribution of complex refractive index. This monomorphous decomposition also simplifies the associated inverse problem [22], of recovering the transverse phase distribution of the scattered field from noninterferometric measurements of one of more intensity distributions over planes perpendicular to the optic axis. This phase-retrieval problem, aided by the previously defined monomorphous decomposition, is the core problem tackled in the present paper.

We close this Introduction with a brief outline of the remainder of the paper. The next section of the paper contains an overview of the so-called "homogeneous" or "monomorphous" version of the TIE [8] and related approaches for phase retrieval of a paraxial complex monochromatic scalar field from noninterferometric measurements of one or more intensity distributions over planes perpendicular to the optic axis. Section III describes a monomorphous decomposition of a generic complex refractive index and complex wave amplitudes. Section IV presents several versions of monomorphous representation of the TIE and discusses their possible applications in in-line imaging, phase retrieval, and phase-contrast tomography. In Sec. V we test some of the methods developed in Sec. IV using a numerical phantom. Section VI contains a brief summary.

II. MONOMORPHOUS TIE AND THE PROBLEM OF STABILITY OF IN-LINE PHASE RETRIEVAL

Continuity equations epitomize the locality in both space and time of energy flows associated with physical fields. As such, they may be constructed for an extremely wide variety of physical fields, from unbound electron and neutron wave functions through to order-parameter and gravitational fields, from Maxwell and Helmholtz fields through to superfluid and acoustical fields. Continuity equations typically have the generic form of the divergence of a current plus the time derivative (or, more generally, derivative with respect to a given evolution parameter) of an energy density being proportional to a term quantifying sources and sinks. In the absence of both sources and sinks, the corresponding term vanishes and the associated current is a conserved current.

To exemplify the above, we restrict consideration to field quantities that can be well approximated by a complex scalar function Ψ that is coupled to a complex (scaled) scalar potential V, obeying a field equation that is a subset of the following very general class of equations (cf. [27]): $[i\alpha\frac{\partial}{\partial\tau} + \nabla^2 + V + f(|\Psi|) + ig(|\Psi|)]\Psi = 0$. Here, α is a scaling parameter; τ is an evolution parameter which is typically time (e.g., for the time-dependent Schrödinger equation) or propagation distance (e.g., for time-independent beamlike solutions to the paraxial equation of scalar wave optics); ∇^2 is the Laplacian in one, two, or three dimensions; $f(|\Psi|)$ is a real function of the wave-field modulus that represents a nondissipative nonlinearity when the said function is not constant; and $g(|\Psi|)$ is another real function which represents a dissipative nonlinearity for the case where it is not constant. Many key vacuum field equations of scalar physical fields are special cases of the above, including (a) the time-dependent Schrödinger equation in one, two, or three spatial dimensions; (b) the Gross-Pitaevskii equation for Bose-Einstein condensates in 1+1, 2+1, and 3+1 dimensions; (c) the 1+1-D and 2+1-D paraxial (parabolic) equation for monochromatic complex scalar beams of visible light, x rays, electrons, and neutrons [27–29]. For all of the above-mentioned special cases, and assuming that one is in the $V = 0$ vacuum region outside the (compact) scatterer, the stated general class of field equations implies the continuity equation $\frac{\alpha}{2}\frac{\partial I}{\partial\tau} + \nabla\cdot(\mathrm{I}\nabla\varphi) = -\mathrm{I}\,g(\sqrt{I})$ where $I = |\Psi|^2$ denotes probability density or intensity, and $\varphi = \arg\Psi$ denotes the wave-field phase. The current density, a vector field that is everywhere proportional to $I\nabla\varphi$, is a conserved current if $g(|\Psi|)$ vanishes, as will be the case in the absence of any dissipative nonlinearities. Note that the nondissipative nonlinearity $f(|\Psi|)$ has no influence on the continuity equation [28].

Irrespective of whether or not $g(|\Psi|)$ vanishes, the continuity equation can be the basis for the inverse problem of phase retrieval, which in the present scenario is the problem of determining $\varphi = \arg\Psi$ given measurements of $I = |\Psi|^2$ over some subset of the vacuum region for which $V = 0$. Given these measurements, which should be such that both I and $\frac{\partial I}{\partial\tau}$ can be estimated over some suitable surface or volume, together with the fact that α is by assumption a known constant and g is a known function, the continuity equation is a second-order elliptic partial differential equation in the unknown phase $\varphi = \arg\Psi$. When considered in the context of the phase-retrieval problem, the continuity equation is termed a *transport-of-intensity equation*, the 2+1-dimensional nondissipative form for which was written down for monochromatic paraxial wave optics by Teague [2]: $k\frac{\partial I}{\partial z} + \nabla\cdot(\mathrm{I}\nabla\varphi) = 0$, where $k = \frac{2\pi}{\lambda}$ is the wave number corresponding to the radiation wavelength λ, z is the propagation distance (evolution parameter) along the optic axis, and ∇ is the gradient operator in two-dimensional planes perpendicular to the optic axis. If one ignores that fact that its potential for phase retrieval was not recognized at the time, the corresponding transport-of-intensity equation for the 3+1-dimensional Schrödinger equation *in vacuo* dates back at least as far as the 1926 paper by Madelung [30], on the "hydrodynamic" formulation of nonrelativistic quantum mechanics. Provided that the solution to the TIE exists and is robust with respect to imperfections in the input intensity data [31], reconstruction of $\varphi = \arg\Psi$ over a given region outside the object may be combined with the direct or indirect measurement of $|\Psi| = \sqrt{I}$ over the same region, to recover the full complex wave function Ψ over the region. This "first" inverse problem (i.e., determining $\varphi = \arg\Psi$ given measurements of $I = |\Psi|^2$) then gives maximal knowledge (modulo the effects of finite spatial resolution) of the information encoded by the scatterer on the scattered complex field; this information can then be input into the "second" inverse problem of reconstructing information regarding the compact complex scattering potential V, given the reconstructed scattered field Ψ.

To exemplify the generality outlined above, we work with Teague's TIE and apply it to the case of phase retrieval in paraxial x-ray imaging. In this context, most methods for phase retrieval using the TIE require multiple x-ray projection images to be acquired under appropriately varied conditions, in order to reconstruct the phase and intensity distributions in the object plane. Suitable projection images can be collected at two or more different sample-to-detector distances [2] or at different x-ray energies [32]. Known exceptions to this rule, where a single image per view angle is sufficient for an exact reconstruction, are represented by the following three cases.

(1) Conventional (or "contact") transmission x-ray imaging and Computed tomography (CT), which can be viewed as a limit case of in-line imaging, in which the sample-to-detector distance is negligibly small. Here x-ray refraction effects do not contribute to the registered images and as a result only the (projection of the) imaginary part $\beta(\mathbf{r})$ of the complex refractive index $n(\mathbf{r}) = 1 - \delta(\mathbf{r}) + i\beta(\mathbf{r})$, $\mathbf{r} = (x,y,z)$, which is responsible for differential absorption of x-ray in the sample, is reconstructed.

(2) The opposite case is represented by the so-called pure-phase objects which exhibit negligible absorption at the x-ray energies used in the experiment. Here only the (projection of the) real decrement $\delta(\mathbf{r})$ of the complex refractive index contributes to the image contrast and can be reconstructed in in-line imaging experiments.

(3) Finally, there is a class of samples characterized by a fixed proportionality relationship between the real and imaginary parts of the refractive index decrement [8]:

$$\delta(\mathbf{r})/\beta(\mathbf{r}) = \gamma, \quad (1)$$

where γ does not depend on $\mathbf{r}$. Obviously, this relationship reduces the number of unknown functions from two to just one (assuming that γ is known *a priori*) and therefore a single projection is sufficient for the reconstruction of both intensity and the phase. Such objects are sometimes also called "monomorphous" [33]. They include, for example, "homogeneous" samples which consist predominantly of a single material whose density may vary spatially. In fact, the above classes (1) and (2) can be viewed as special cases of class (3) with $\gamma = 0$ and $\gamma = \infty$, respectively.

We consider here the case of a plane monochromatic incident wave of unit intensity propagating along the optic axis z. The object that is being imaged is located in the half space $z < 0$ and is characterized by the distribution of its complex refractive index, which is assumed to be time independent. The value of Eq. (1) for TIE-based phased retrieval is in the following relationship (valid under the projection approximation) between the phase, $\phi_0(x,y) = -k\int_{-\infty}^{0}\delta(x,y,z)dz$, and intensity, $I_0(x,y) = \exp[-2k\int_{-\infty}^{0}\beta(x,y,z)dz]$, distributions in the object plane:

$$\phi_0(x,y) = (\gamma/2)\ln I_0(x,y). \quad (2)$$

Therefore, for the purpose of phase retrieval it does not matter if Eq. (1) holds, as long as the (weaker) Eq. (2) is satisfied. Moreover, it turns out that in order to derive the "monomorphous" version of the general TIE, it is sufficient to require the constant proportionality only between the gradients of the logarithm of intensity of the transmitted wave and the logarithm of its phase across the object plane:

$$\nabla\phi_0(x,y) = (\gamma/2)\nabla I_0(x,y)/I_0(x,y), \quad (3)$$

where $\nabla \equiv (\partial_x,\partial_y)$ is the two-dimensional (2D) transverse gradient operator. Obviously, Eq. (3) is a weaker requirement compared to that of the proportionality of the logarithm of intensity and the phase themselves, as in Eq. (2). Substituting Eq. (3) into the generic TIE [1,2], one arrives at the following "monomorphous" form of the TIE [8]:

$$I_R(x,y) = I_0(x,y) - \gamma\, R/(2k)\,\nabla^2 I_0(x,y), \quad (4)$$

where $I_R(x,y)$ is the intensity distribution in the detector (image) plane $z = R$.

Given the inherent sensitivity of the phase-retrieval methods based on the TIE to noise in the input images, the technique proposed in [8] on the basis of Eq. (4) was an important development as it allowed a stable and quantitatively accurate recovery of the phase from a single in-line image containing realistic amounts (several percent) of noise. To date, this "monomorphous TIE" method appears to be by far the most successful one in x-ray imaging applications of the TIE. The remarkable stability of the method has been explained by the fact that it optimally combines the sensitivity of the phase contrast to high-spatial-frequency components of the transmitted complex amplitude, provided by the second term on the right-hand side (r.h.s.) of Eq. (4), with the complementary sensitivity [provided by the first term on the r.h.s. of Eq. (4)] of the absorption contrast to the low-frequency components. Mathematically, when $\gamma>0$, this equation corresponds to a strictly positive partial differential operator whose spectrum is separated from zero and, therefore, it does not have zeros in the corresponding contrast transfer function at low spatial frequencies. However, this useful property can only be attained for a special class of objects (transmitted complex amplitudes), namely, those satisfying Eq. (3). Samples consisting of a single material obviously possess this property [8], as well as samples consisting of light chemical elements with $Z<10$, if the x-ray energy of the incident radiation is approximately between 60 and 500 keV [34]. The latter case corresponds to the fact that, for suitably high x-ray energy, the scattering properties of most light-element materials can be well approximated by the corresponding electron density, with no nuancing needed to account for the effects of atomic, chemical, or nuclear structure: At sufficiently high energies almost all light-element materials become one material, namely "electron jelly," as far as x-ray scattering is concerned [34,35]. Due to the proportionality of the attenuation and phase shifts generated by samples obeying Eq. (3), the phase can be retrieved from a single defocused image [8], which is of course an extremely useful property as it allows one to avoid experimental problems related to image coregistration due to possible instabilities of the incident beam, optical elements, and/or the sample, as well as significantly simplify the data acquisition compared to phase-retrieval methods requiring the acquisition of multiple images. The applicability of this method to monomorphous samples only is the main limitation of the method.

As a further natural extension of the "monomorphous" condition represented by Eq. (3), we would like to mention the following theorem proven in [29]:

For an arbitrary pair of suitably well-behaved functions (I_0,ϕ_0) in a domain Ω in a 2D plane (x,y), there exists a function ψ such that $\nabla\psi_0(x,y) = I_0(x,y)\nabla\phi_0(x,y)$, if and only if

$$\nabla I_0(x,y) \times \nabla\phi_0(x,y) \equiv 0, \quad (5)$$

(where "$\times$" denotes the vector product), i.e., if the vector fields $\nabla\phi_0$ and ∇I_0 are parallel to each other everywhere in Ω (here a vector of zero length is considered parallel to any other vector). Note that Eq. (3) means that the vectors $\nabla\phi_0$ and ∇I_0 are parallel everywhere, and the ratio of their lengths is equal exactly to $(\gamma/2)/I_0(x,y)$ at each point. Therefore, Eq. (5) is indeed a direct generalization of Eq. (3). The above equivalence of Eq. (5) and the existence of gradient function ψ such that $\nabla\psi_0(x,y) = I_0(x,y)\nabla\phi_0(x,y)$ means that Eq. (5) is a sufficient condition for the well-known method for solution of the TIE originally proposed by Teague [2] and later developed in [36] and used in many other publications. Note, however that, unlike the phase retrieval using the homogeneous TIE, Eq. (4), Teague's method, being based on the generic TIE, requires at least two different intensity images acquired, e.g., at different defocus distances. As a consequence, Teague's method does not deliver any extra stability to the solution of the TIE compared to other, more generic methods. It does lead, however, to a form of "single-step" phase-contrast CT reconstruction formula [37] that generalizes the result originally obtained by Bronnikov [38,39] and later extended by others [40,41].

A number of different methods for TIE-based phase retrieval have been proposed and tested for generic (non-monomorphous) objects [9–20]. These methods usually require more than one image collected either at different defocus distances [2] or at the same distance but at different radiation wavelengths [12]. While being formally mathematically well posed [6], these methods suffer from the generic low-frequency instability inherent to phase retrieval using the TIE. As mentioned above, this instability is tightly related to the requirement for the propagation contrast to be low in order for the TIE approximation to be valid. Although quantitatively accurate phase retrieval from multiple defocused images of a generic object has been robustly demonstrated in both the visible light region [24,25] and also for paraxial electron wave fields in the context of transmission electron microscopy [42,43], as far as we are aware this success has never been reproduced convincingly with x rays, despite a number of attempts. It appears that one of the main difficulties in performing accurate TIE-based phase retrieval from multiple defocused x-ray images is in the variation of the incident illumination, which tends to be more pronounced for x-ray sources compared to high-quality visible light sources. While the change in the incident intensity can often be at least partially compensated by using appropriate "flat field" images (collected at the same defocus distances but without the sample), the change in the phase distribution of the incident illumination generally cannot be corrected for, except, perhaps, for the lowest tilt and defocus aberrations that can be detected and corrected in software by comparing the positions of image boundaries. The other aberrations of the illuminating beam usually end up as artifacts in the reconstructed phase, which often overwhelm the true signal from the sample. Another difficulty, which makes x-ray TIE imaging using multiple defocused images significantly more difficult than the corresponding problem using either visible light or electrons, is the "aspect ratio problem" and the associated difficulty in image registration: for visible light the defocus distance between adjacent planes requires a small defocus (measured relative to the pixel width), and for electrons the required defocus is moderate but not excessive, but for x-ray imaging the required defoci relative to pixel width can be massive (e.g., defocus distances on the order of meters are typical for phase-contrast imaging of biomedical specimens, which is five orders of magnitude larger than typical pixel sizes of tens of microns).

The above issues regarding noise robustness are fairly standard for reconstructive imaging under low signal-to-noise conditions. One of the most powerful tools for dealing with this type of problem is the use of *a priori* information. Obviously, in order to maximize the usability of a phase-retrieval method one would generally want to minimize the amount of *a priori* information required for successful performance of the method, and, whenever possible, use only generic information, such as e.g., the positivity of the real and imaginary parts of the complex refractive index. Given the success of the monomorphous TIE method, it appears useful to try to extend its positive traits—namely, the use of absorption contrast for regularizing phase retrieval at low spatial frequencies—to generic samples. Even though for generic samples one cannot assume that the ratio of the real to imaginary part of the refractive index is constant throughout the sample, it should be possible in most cases to estimate the upper and lower limits of this ratio, e.g., from *a priori* knowledge of the expected material constituents of the sample. By constraining this ratio one should be able to eliminate at least some of the phase artifacts, thus improving the stability of the phase retrieval. This constitutes the basic idea of the method presented below.

III. MONOMORPHOUS DECOMPOSITION OF COMPLEX REFRACTIVE INDEX AND COMPLEX WAVE AMPLITUDE

The Maxwell equations imply that the interaction of a linear isotropic nonmagnetic static object with an incident monochromatic scalar x-ray beam is determined by a three-dimensional (3D) distribution of its complex refractive index:

$$n(\mathbf{r};\lambda) = 1 - \delta(\mathbf{r};\lambda) + i\beta(\mathbf{r};\lambda), \tag{6}$$

where $\mathbf{r} = (x,y,z)$ is the Cartesian spatial coordinate and λ is the x-ray wavelength, and $n(\mathbf{r};\lambda)$ is by assumption slowly varying over the characteristic length scale λ [22]. We have adopted the definition according to which an object is called "monomorphous" if the ratio $\gamma(\lambda) \equiv \delta(\mathbf{r};\lambda)/\beta(\mathbf{r};\lambda)$ is independent from $\mathbf{r}$ throughout the sample. We will omit below the wavelength argument λ for brevity.

Let us check now that for any given fixed energy an arbitrary complex refractive index distribution can be represented as a sum of two monomorphous ones, or more precisely that for any pair of constants γ_1 and γ_2, $\gamma_1 \neq \gamma_2$, there exist such real-valued functions $\beta_1(\mathbf{r})$ and $\beta_2(\mathbf{r})$ such that

$$-\delta(\mathbf{r}) + i\beta(\mathbf{r}) \equiv \beta_1(\mathbf{r})(-\gamma_1 + i) + \beta_2(\mathbf{r})(-\gamma_2 + i). \tag{7}$$

Indeed, it is easy to verify that Eq. (7) is satisfied, provided that

$$\begin{aligned} \beta_1(\mathbf{r}) &= [\delta(\mathbf{r}) - \gamma_2\beta(\mathbf{r})]/(\gamma_1 - \gamma_2) \\ \beta_2(\mathbf{r}) &= [\delta(\mathbf{r}) - \gamma_1\beta(\mathbf{r})]/(\gamma_2 - \gamma_1). \end{aligned} \tag{8}$$

As we see, Eq. (7) has a unique solution for any pair of constants γ_1 and γ_2, such that $\gamma_1 \neq \gamma_2$. However, normally for x rays $\beta(\mathbf{r}) > 0$ and $\delta(\mathbf{r}) > 0$, and therefore it is natural to demand that both $\beta_1(\mathbf{r})$ and $\beta_2(\mathbf{r})$ are positive everywhere (assuming that both γ_1 and γ_2 are positive as well). Therefore, if, for example, $0 < \gamma_1 < \gamma_2$, it is easy to verify that the requirement for $\beta_1(\mathbf{r})$ and $\beta_2(\mathbf{r})$ to be positive leads to the following condition:

$$\gamma_1 \leqslant \delta(\mathbf{r})/\beta(\mathbf{r}) \leqslant \gamma_2 \quad \text{for all } \mathbf{r} \text{ inside the sample.} \tag{9}$$

The condition given by Eq. (9) implies a strategy where a monomorphous decomposition of an unknown object should have the first monomorphous component with the minimal $\delta(\mathbf{r})/\beta(\mathbf{r})$ ratio for all materials possibly present in the sample, while the second component should have the maximal $\delta(\mathbf{r})/\beta(\mathbf{r})$ ratio. In this context, it is already clear that the two monomorphous components establish an *a priori* "envelope" for the reconstructed values of the $\delta(\mathbf{r})/\beta(\mathbf{r})$ ratio, thus preventing large erroneous phase oscillations which otherwise might have appeared due to inconsistencies in the measured image intensities.

Let the monochromatic plane incident x-ray wave $I_{\rm in}^{1/2}\exp(ikz)$ with intensity $I_{\rm in}$ and wave vector $k = 2\pi/\lambda$ propagate along the optic axis z. Given the monomorphous decomposition equation (7) of the sample, we can represent the transmitted intensity in the object plane $z = 0$ as

$$I_0(x,y) = I_{\rm in}\, Q_1(x,y)\, Q_2(x,y), \qquad (10)$$

where

$$Q_j(x,y) = \exp\left[-2k\int \beta_j(x,y,z)dz\right], \quad j = 1,2, \qquad (11)$$

are the transmittances corresponding to the two monomorphous components. The corresponding transmitted phase in the object plane is then

$$\phi_0(x,y) = \phi_1(x,y) + \phi_2(x,y), \qquad (12)$$

where

$$\phi_j(x,y) = -k\int \delta_j(x,y,z)dz) = (\gamma_j/2)\ln Q_j(x,y), \quad j = 1,2. \qquad (13)$$

Note that the monomorphous decomposition, Eqs. (10)–(13), of a transmitted complex amplitude $U_0(x,y) \equiv I_0^{1/2}(x,y)\exp[i\phi_0(x,y)]$ can in principle be performed without a reference to the monomorphous decomposition equation (7) of the object, using instead some "abstract" transmission functions Q_1 and Q_2. Indeed, for any given pair of functions $I_0(x,y)$ and $\phi_0(x,y)$, and any pair of constants $0 < \gamma_1 < \gamma_2$, such that

$$\gamma_1 \leqslant 2\phi_0(x,y)/b_0(x,y) \leqslant \gamma_2 \quad \text{for all} \quad (x,y), \qquad (14)$$

where $b_0(x,y) \equiv \ln[I_0(x,y)/I_{\rm in}]$, there exists a unique pair of functions $Q_1(x,y)$ and $Q_2(x,y)$, such that Eqs. (10) and (12) hold with $\phi_j(x,y) = (\gamma_j/2)\ln Q_j(x,y)$, $j = 1,2$. It is straightforward to verify that the required functions are given by

$$\ln Q_1(x,y) = [2\phi_0(x,y) - \gamma_2 b_0(x,y)]/(\gamma_1 - \gamma_2)$$
$$\ln Q_2(x,y) = [2\phi_0(x,y) - \gamma_1 b_0(x,y)]/(\gamma_2 - \gamma_1). \qquad (15)$$

Condition equation (14) ensures that the functions $Q_j(x,y)$ satisfy the inequalities

$$I_0(x,y)/I_{\rm in} \leqslant Q_j(x,y) \leqslant 1 \quad \text{for all} \quad (x,y),\ j = 1,2. \qquad (16)$$

The limit cases $Q_1(x,y) = 1$, $Q_2(x,y) = I_0(x,y)/I_{\rm in}$, and $Q_1(x,y) = I_0(x,y)/I_{\rm in}$, $Q_2(x,y) = 1$, correspond to monomorphous cases with $\phi_0(x,y) = (\gamma_2/2)b_0(x,y)$ and $\phi_0(x,y) = (\gamma_1/2)b_0(x,y)$, respectively (Fig. 1).

IV. TRANSPORT OF INTENSITY EQUATION IN MONOMORPHOUS REPRESENTATION

The TIE expresses intensity distribution in a plane $z = R$ downstream from the object plane $z = 0$, as a function of the intensity and phase distributions in the object plane [1,2]:

$$I_R(x,y) = I_0(x,y) - (R/k)\nabla\cdot[I_0(x,y)\nabla\phi_0(x,y)]. \qquad (17)$$

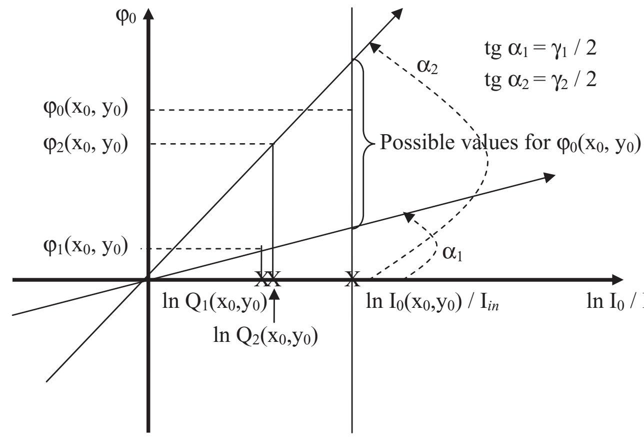

FIG. 1. Illustration of the constraints imposed by *a priori* knowledge of coefficients γ_1 and γ_2 on the range of possible phase values corresponding to a given intensity value.

Substituting the monomorphous representation Eqs. (10)–(13) for the intensity and phase in the object plane into Eq. (17) and omitting all function arguments for brevity, we obtain

$$I_R = [1 - R\gamma_1/(2k)\nabla^2]I_0 - R(\gamma_2 - \gamma_1)/(2k)I_{\rm in} \times \nabla\cdot[Q_1\nabla Q_2]. \qquad (18)$$

This equation should be considered together with Eq. (10), $I_0 = I_{\rm in}Q_1Q_2$. If we express $Q_1 = I_0/(I_{\rm in}Q_2)$ from Eq. (10) and substitute it into Eq. (18), the latter equation becomes

$$I_R = [1 - R\gamma_1/(2k)\nabla^2]I_0 - R(\gamma_2 - \gamma_1)/(\gamma_2 k)\nabla\cdot[I_0\nabla\varphi_2]. \qquad (19)$$

This equation can be solved for the unknown phase φ_2 if intensity distributions in the object and image planes, I_R and I_0, are known. Subsequently, Q_2 can be easily calculated as $Q_2 = \exp(2\phi_2/\gamma_2)$; then Q_1 can be obtained as $Q_1 = I_0/(I_{\rm in}Q_2)$. This gives us $\phi_1 = (\gamma_1/2)\ln Q_1$ and finally $\varphi_0 = \varphi_1 + \varphi_2$. Unfortunately, Eq. (19) is even worse in terms of numerical stability than the original TIE, Eq. (17). In order to emulate the favorable stability properties of the monomorphous TIE we shall rearrange Eq. (18) as follows:

$$2I_R - [1 - (R\gamma_1/k)\nabla^2]I_0 = I_{\rm in}Q_1Q_2 - [R(\gamma_2 - \gamma_1)/k]I_{\rm in}\nabla\cdot[Q_1\nabla Q_2]. \qquad (20)$$

The last equation does possess the desired mathematical stability property with respect to the unknown function Q_2 (if Q_1 is known). Indeed, it is easy to see that (a) the first term on the r.h.s. of Eq. (20) represents a multiplication of function Q_2 by a function $I_{\rm in}Q_1$ which is positive everywhere; (b) the second term on the r.h.s. of Eq. (20) represents a non-negative partial differential operator applied to Q_2. Hence, the whole of the r.h.s. of Eq. (20) represents a strictly positive operator applied to Q_2 (i.e., the spectrum of this operator is separated from zero). Therefore, this operator is invertible and the norm of its inverse (determined by the inverse of the lower bound of the spectrum of the direct operator) is finite; i.e., Eq. (20) is mathematically well posed and stable.

We can solve Eq. (20) in combination with Eq. (10) iteratively. We can take, for example, $Q_1^{(0)} \equiv 1$ as an initial guess (a similar technique can be applied with $Q_1^{(0)} \equiv I_0$, and with other choices). This transforms Eq. (20) into a conventional monomorphous TIE which can be explicitly solved:

$$Q_2^{(0)} = I_{\rm in}^{-1}[1 - R\gamma_2/(2k)\nabla^2]^{-1} I_R. \quad (21)$$

In other words, the zero-order approximate solution is given here by the monomorphous distribution with $2\phi_0^{(0)}(x,y) = \gamma_2 b_0(x,y)$. Subsequent iterations are performed by evaluating $Q_1^{(n)} = I_0/(I_{\rm in} Q_2^{(n-1)})$, substituting this into Eq. (20) and solving the resultant equation:

$$Q_2^{(n)} = \left[I_{\rm in} Q_1^{(n)} - Rk^{-1}(\gamma_2 - \gamma_1) I_{\rm in} \times \nabla \cdot \left(Q_1^{(n)} \nabla\right)\right]^{-1} \left[2I_R - (1 - Rk^{-1}\gamma_1 \nabla^2) I_0\right]. \quad (22)$$

The latter solution can be implemented numerically, e.g., using the full multigrid method [44]. Equation (22) has stability properties similar to those of the monomorphous TIE due to the fact that $Q_1^{(n)}(x,y) \geqslant \text{const} > 0$ at any n.

The issue of convergence of the iterative process is not obvious, and we can only state that we have observed proper convergence in the numerical examples that we have considered so far in the absence of noise. If the input data contain some noise, then the iterative process displays the usual semiconvergent behavior; i.e., it converges for several iterations before beginning to diverge. In this context it becomes important to find a reliable "stopping criterion" in order to prevent the process from diverging. For example, one can stop the iterations when the difference between successive iterations becomes smaller than the noise level. Assuming Poisson noise, this leads to the following criterion:

$$||I_0^{1/2}\left[1 - Q_2^{(n)}/Q_2^{(n-1)}\right]||_2 > \sigma_{bckg}, \quad (23)$$

where σ_{bckg} is the standard deviation of the Poisson distribution in a sample-free area of the image (background) and $\|\,\|_2$ denotes the normalized root-mean-square metric.

A simpler version of the monomorphous TIE decomposition can be derived for weakly absorbing objects, when the approximation $I_0(x,y)/I_{\rm in} = \exp b_0(x,y) \cong 1 + b_0(x,y)$, $b_0(x,y) = -2k\int_{-\infty}^{0} \beta(x,y,z)dz$, can be applied, i.e., when $|\ln[I_0(x,y)/I_{\rm in}]| \ll 1$. In this case, Eq. (11) can also be linearized:

$$Q_j(x,y) \cong 1 + b_j(x,y),$$
$$\text{where } b_j(x,y) = -2k\int \beta_j(x,y,z)dz, \quad j = 1,2, \quad (24)$$

because $|b_j(x,y)| \leqslant |b_0(x,y)| \ll 1$. Substituting Eq. (24) into Eq. (18) and discarding the second-order terms (containing the products $b_i b_j$ or their derivatives), we obtain after simple algebraic transformations,

$$K_0 \equiv I_0/I_{\rm in} - 1 = b_1 + b_2,$$
$$K_R \equiv I_R/I_{\rm in} - 1 = [1 - R\gamma_1/(2k)\nabla^2]b_1 + [1 - R\gamma_2/(2k)\nabla^2]b_2, \quad (25)$$

where $K_0(x,y)$ and $K_R(x,y)$ are the experimentally measurable "contrast functions" in the object and image planes, respectively. As can be seen from Eq. (25), in the case of weakly absorbing samples (note that the phase shifts can in principle be large), the TIE becomes linear with respect to the absorption contributions of the two monomorphous components. Note that the equations for the zero-order (constant) Fourier components of b_1 and b_2 are underdetermined, as for these components the first and the second line of Eq. (25) give the same results, in agreement with the conservation of total intensity in the course of free-space propagation of light. Therefore, we can always assume without loss of generality, that, for example, the integral of b_2 over the image is equal to zero and the integral of b_1 is equal to the integral of $I_0/I_{\rm in} - 1$, i.e., to the total absorption in the sample.

The issue of numerical solution of Eq. (25) is still not straightforward in general. Expressing b_1 from the first line of Eq. (25) and substituting the result into the second line leads to

$$K_R - [1 - R\gamma_1/(2k)\nabla^2]K_0 = R(\gamma_1 - \gamma_2)/(2k)\nabla^2 b_2. \quad (26)$$

Unfortunately, this equation is numerically unstable, similarly to Eq. (19). However, compared to Eq. (19), Eq. (26) is easier to regularize (the fact that the integral of b_2 over the image is equal to zero can be used explicitly for that purpose, as shown below) and to solve. Collecting multiple images $I_R(x,y)$ at different propagation distances $R = R_k$ can also help in constructing a stable solution [24].

A regularized iterative approach, similar to the one given by Eq. (22), can be devised by choosing an initial approximation $b_1^{(0)}(x,y) = f(x,y)$, where $f(x,y) = K_0(x,y)$ or $f(x,y) \equiv 0$ (or some *a priori* plausible distribution), and then iterating

$$b_2^{(k)} = [1 - R\gamma_2/(2k)\nabla^2]^{-1}\left\{K_R - [1 - R\gamma_1/(2k)\nabla^2]b_1^{(k-1)}\right\},$$
$$b_1^{(k)} = K_0 - b_2^{(k)}. \quad (27)$$

By substituting the second line of Eq. (27) into the first one, it is possible to verify that this iterative scheme leads to the following series solution:

$$b_2 = K_0 + \sum_{n=0}^{\infty} \mathbf{A}^n\{\mathbf{B}K_R - K_0\}, \quad (28)$$

where $\mathbf{A} = [1 - R\gamma_1/(2k)\nabla^2][1 - R\gamma_2/(2k)\nabla^2]^{-1}$ and $\mathbf{B} = [1 - R\gamma_2/(2k)\nabla^2]^{-1}$. Operator $\mathbf{A}$ can be expressed as

$$\mathbf{A}f = \iint \exp[i2\pi(x\xi + y\eta)]\hat{f}(\xi,\eta) \times \frac{1 + \pi\lambda R\gamma_1(\xi^2 + \eta^2)}{1 + \pi\lambda R\gamma_2(\xi^2 + \eta^2)} d\xi d\eta. \quad (29)$$

Therefore, it is bounded in the space of square-integrable functions L_2 and its norm $\|\mathbf{A}\|_2$ does not exceed $[1 + \pi\lambda R\gamma_1(\xi_{\min}^2 + \eta_{\min}^2)]/[1 + \pi\lambda R\gamma_2(\xi_{\min}^2 + \eta_{\min}^2)]$. Let us consider for simplicity a square image Ω with the linear size a. Then the Fourier integral in Eq. (29) can be replaced by the corresponding Fourier series. If we restrict the domain $D(\mathbf{A};\Omega)$ of functions, on which operator $\mathbf{A}$ acts, to the subspace $D_1(\mathbf{A};\Omega) = D(\mathbf{A};\Omega)\backslash\{\mathbf{1}\}$ equal to the orthogonal complement to constant functions, then we will have $\|\mathbf{A}\|_2 \leqslant [1 + \pi\lambda R\gamma_1 a^{-2}]/[1 + \pi\lambda R\gamma_2 a^{-2}] < 1$ on that subspace (as the lowest order of Fourier coefficients is now equal to 1). This estimate guarantees the uniform and absolute convergence of the series in Eq. (28) for any $f \in D_1(\mathbf{A};\Omega)$. We have explained

FIG. 2. Initial intensity (a), and phase (b), distributions in the object plane.

above that it can be assumed without loss of generality that the zero-order Fourier coefficient of b_2 is equal to zero. As the matrix of the operator **A** is diagonal in the Fourier space representation [see Eq. (29)], we can now find b_2 by solving Eq. (28) on $D_1(\mathbf{A};\Omega)$. The series in Eq. (28) then converge to

$$b_2 = 2k/[R(\gamma_1-\gamma_2)]\nabla^{-2}\{K_R - [1-R\gamma_1/(2k)\nabla^2]K_0 - c_0\}, \quad (30)$$

where c_0 is a constant equal to the average of the function $K_R - [1-R\gamma_1/(2k)\nabla^2]K_0$ over the image Ω. Once b_2 is found, b_1 can be easily found too from the first line of Eq. (25). The phase function can then be obtained as $\varphi_0(x,y) = (\gamma_1/2)b_1(x,y) + (\gamma_2/2)b_2(x,y)$. Note that the solution given by Eq. (30) corresponds to a direct regularization of Eq. (26). However, as shown in the next section, a truncation of the series in Eq. (28) [i.e., a finite number of iterations according to Eq. (27)] may provide a more robust solution compared to Eq. (30) in the presence of noise and experimental measurement errors (e.g., due to the changes in the incident illumination) in the input data (measured image intensities).

V. NUMERICAL TESTS

In this section we present the results of a test of one of the phase-retrieval algorithms developed in the previous section, Eq. (27). It is well known that the single-image TIE phase-retrieval method for objects (including homogeneous objects) obeying Eq. (3) ("TIE-Hom") [8] is very stable and accurate when applied to monomorphous objects (corresponding to monomorphous complex amplitude distributions in the object plane). The "monomorphous decomposition" method developed in the present paper obviously reduces to TIE-Hom in the monomorphous case (here one can set $Q_1 = 1$ or $Q_2 = 1$). In order to investigate the most difficult case for our method, we performed a test using a complex amplitude in the object plane that cannot be approximated by a monomorphous one. The relevant intensity and phase distributions are shown in Fig. 2 (each image had 1024×1024 pixels). Obviously, here the logarithm of the intensity and the phase are not proportional to each other, so the complex wave amplitude is not monomorphous. The ratio $\gamma(x,y) = 2\varphi_0(x,y)/\ln I_0(x,y)$ varied between $\gamma_{\min} = 12.1$ and $\gamma_{\max} = 39.6$ in this example. For the reconstruction below, we chose $\gamma_1 = 10$ and $\gamma_2 = 50$, so that $\gamma_1 \leqslant \gamma_{\min} < \gamma_{\max} \leqslant \gamma_2$. We assigned the following

FIG. 3. In-line image intensity distribution.

physical parameters to the images: Linear size was set to $a = 1$ cm, the range of intensity values was approximately (0.85, 0.9), the range of phase values was (–2.2, –1), and the wavelength was 1 Å (corresponding to hard x rays). We then calculated an in-line free-space-propagated image at the object-to-image distance $z = 10$ m by numerically evaluating the corresponding Fresnel integrals with the help of the well-tested X-TRACT software [45]. The corresponding image is shown in Fig. 3. For such "ideal" (noise-free) images, the phase distribution in the object plane can be retrieved with high accuracy using a conventional TIE, Eq. (17). We have verified this fact using an implementation of the general TIE solution available in X-TRACT. The relative l_2 error between the original and the reconstructed phase distributions, calculated according to the usual formula,

$$d_2(\varphi_0^{\rm rec},\varphi_0^{\rm true}) = \frac{\|\varphi_0^{\rm rec}-\varphi_0^{\rm true}\|_2}{\|\varphi_0^{\rm true}\|_2} = \frac{\left\{\sum_m\sum_n\left[\varphi_0^{\rm rec}(m,n)-\varphi_0^{\rm true}(m,n)\right]^2\right\}^{1/2}}{\left\{\sum_m\sum_n\left[\varphi_0^{\rm true}(m,n)\right]^2\right\}^{1/2}}, \quad (31)$$

was equal to 0.027 and the visual difference between the two images was imperceptible. We then added 1% (relative to the average image intensity) of Poisson noise to the intensity distributions in the object and image planes. The noisy intensity distribution in the object plane is shown in Fig. 4. Even with this relatively small amount of noise, the performance of the conventional TIE phase retrieval (from

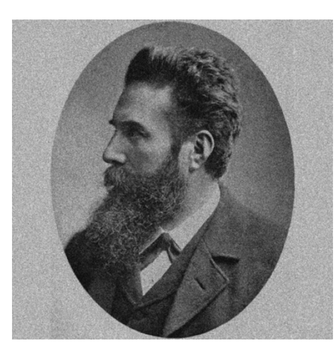

FIG. 4. Object plane intensity with 1% noise.

FIG. 5. Phase distribution in the image plane reconstructed using conventional TIE, Eq. (17), from two images with 1% noise (a); the same reconstructed distribution with the first 21 low-order Zernike components subtracted (b).

images at two different propagation distances) deteriorated very significantly; see Fig. 5. It is obvious from Fig. 5(a) that there were strong errors in the low spatial frequencies (low-order aberrations). However, when the low-order components corresponding to the first 21 circular Zernike polynomials were subtracted from the reconstructed image, the higher-order error terms became apparent [Fig. 5(b)]. The relative l_2 error $d_2(\varphi_0^{\mathrm{rec}},\varphi_0^{\mathrm{true}})$ between the original and the reconstructed phase distributions was equal to 3.19 here; i.e., it increased 118 times compared to the reconstruction from the noise-free images. Such a dramatic dependence of the reconstruction error on the noise in the input data is a well-known property of the TIE phase retrieval from images collected at different propagation distances (see e.g., [8,9,24]).

We then applied the iterative reconstruction algorithm defined by Eq. (27) above to the intensity distributions in the object and image planes with 1% noise. The results are shown in Fig. 6. Even though visually these reconstructions do not look much better (if at all) than the reconstructions in Fig. 5 obtained using the conventional TIE, in fact the phase distributions in Fig. 6 contain a much smaller amount of low-order aberrations and the overall error $d_2(\varphi_0^{\mathrm{rec}},\varphi_0^{\mathrm{true}})$ between the original and the reconstructed phase distributions was much smaller here: 0.883 and 0.642 for the distributions in Figs. 6(a) and 6(b), respectively. Thus, the error in the phase reconstructed with Eq. (27) was almost five times smaller compared to the reconstruction using the conventional TIE. We have also specifically compared the accuracy of the reconstruction of the low-order spatial frequencies of the phase distribution using the two methods. The sum of absolute errors in the first 21 Zernike coefficients between the original phase distribution and the one reconstructed using the conventional TIE was 4.144, while that error was equal to 1.081 and 0.991 in the images obtained using Eq. (27) after two and 20 iterations, respectively; recall, in this context, that the Zernike polynomials form a convenient orthonormal set over a disk-shaped region [31].

FIG. 6. Phase distribution in the image plane reconstructed according to Eq. (27) from two images with 1% noise, after two iterations (a), and after 20 iterations (b).

TABLE I. Relative l_2 errors between the original and the reconstructed phase distributions obtained using Eq. (27) with different number of iterations. The input data contained 1% Poisson noise (column 2) and an additional 1-pixel horizontal shift of the propagated image (column 3).

Number of iterations, Eq. (27)	$d_2(\varphi_0^{\mathrm{rec}},\varphi_0^{\mathrm{true}})$ error (1% noise)	$d_2(\varphi_0^{\mathrm{rec}},\varphi_0^{\mathrm{true}})$ error (1% noise and 1-pixel shift)
2	0.883	0.889
4	0.814	0.826
6	0.770	0.789
10	0.713	0.747
20	0.642	0.718
50	0.576	0.792
100	0579	1.010

The advantage of the method defined by Eq. (27) over the phase retrieval using the conventional TIE was even more obvious in the case of geometrical misalignment between the images in the object and image planes. In order to simulate this problem, we shifted the image-plane intensity distribution by one pixel horizontally with respect to the object-plane intensity. This shift led to the $d_2(\varphi_0^{\mathrm{rec}},\varphi_0^{\mathrm{true}})$ error in the conventional TIE reconstruction increasing by a further 50% from 3.19 (in the case of 1% noise and no shift) to 4.68 (in the case of 1% noise and 1 pixel shift). Remarkably, the accuracy of the reconstruction using Eq. (27) changed by only a few percent as a result of this input data misalignment: $d_2(\varphi_0^{\mathrm{rec}},\varphi_0^{\mathrm{true}})$ changed from 0.883 to 0.889 at 2 iterations, and from 0.642 to 0.718 at 20 iterations (see Table I), the latter one being 6.5 times smaller than the corresponding error in the reconstruction using the conventional TIE.

Figure 7 shows the relative reconstruction error $d_2(\varphi_0^{\mathrm{rec}},\varphi_0^{\mathrm{true}})$ as a function of the number of iterations [according to Eq. (27)]. One can see that the algorithm demonstrates a semiconvergent nature, as expected in the presence of noise and other inconsistencies in the input data. In fact, in this case, the series in Eq. (28) still converges, but the limit no longer corresponds to the "true" (noise-free) phase distribution, because of the mathematical inconsistency of the input data due to the presence of noise and the geometrical misalignment. Therefore, in practice, when the ideal phase distribution is not known, the reconstruction can be stopped, e.g., when the difference between two successive iterations becomes smaller than the noise level in the input data. This stopping criterion performed well in the case of the numerical example considered above.

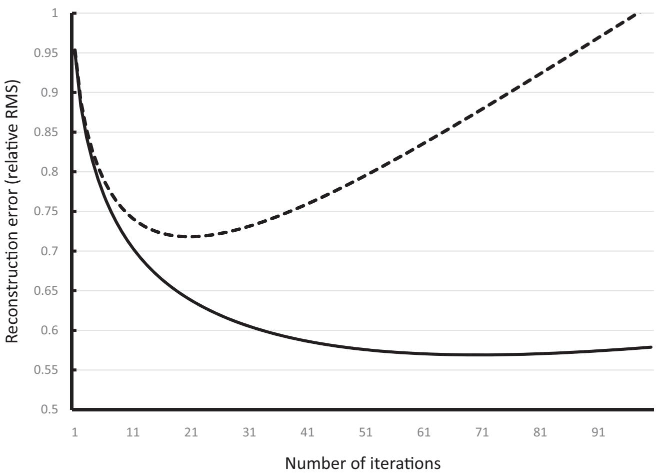

FIG. 7. Reconstruction error as a function of the number of iterations (solid line: 1% noise in input data; dashed line: 1% noise and 1-pixel horizontal shift).

VI. SUMMARY

In this paper, we reviewed several types of objects (defined in terms of the spatial distribution of the complex refractive index) for which the quantitative analysis of in-line phase-contrast images and phase retrieval can be simplified. For monomorphous objects, in particular, the projected distribution of the complex refractive index can be uniquely reconstructed from measurements of in-line image intensity distribution in a single plane orthogonal to the optic axis in the near field [8]. We then demonstrated that an arbitrary pair of 2D distributions of phase and intensity in the object plane can always be represented as a linear combination of two monomorphous pairs of phase and intensity distributions. Such a decomposition of arbitrary complex wave amplitude (or, equivalently, of an arbitrary 3D distribution of the complex refractive index in the case of CT) can be used as a basis for development of "stabilized" versions of phase-retrieval algorithms based on the TIE. In our numerical tests, using a proposed iterative algorithm based on the monomorpous decomposition, the reconstruction of the phase distribution from in-line intensities in the object and image planes has demonstrated an improved stability in the case of the input data containing simulated photon noise and geometrical misalignment. The reconstruction was also quite stable as a function of the number of iterations. As the proposed method appears capable of providing better accuracy in phase retrieval compared to the conventional algorithms, we believe that it can be useful in quantitative 2D phase-contrast imaging and in phase-contrast tomography. The generalization beyond x rays, to a rich variety of additional 2+1-D fields requires either minimal or zero modification to the underpinning TIE, implying that this work can be readily extended to, e.g., paraxial electron and neutron beams, nonlinear optical beams, nonvortical 2+1-D Bose-Einstein condensates, and scalar 2+1-D superfluid systems.

[1] J. M. Cowley, *Diffraction Physics* (Elsevier, Amsterdam, 1995).
[2] M. R. Teague, Deterministic phase retrieval: a Green's function solution, J. Opt. Soc. Am. **73**, 1434 (1983).
[3] F. Roddier, Wavefront sensing and the irradiance transport equation, Appl. Optics **29**, 1402 (1990).
[4] J. P. Guigay, Fourier transform analysis of Fresnel diffraction patterns and in-line holograms, Optik **49**, 121 (1977).
[5] D. Van Dyck and W. Coene, A new procedure for wave function restoration in high resolution electron microscopy, Optik **77**, 125 (1987).
[6] T. E. Gureyev and K. A. Nugent, Phase retrieval with the transport of intensity equation II. Orthogonal series solution for nonuniform illumination, J. Opt. Soc. Am. A **13**, 1670 (1996).
[7] A. Pogany, D. Gao, and S. W. Wilkins, Contrast and resolution in imaging with a microfocus x-ray source, Rev. Sci. Instrum. **68**, 2774 (1997).
[8] D. Paganin, S. C. Mayo, T. E. Gureyev, P. R. Miller, and S. W. Wilkins, Simultaneous phase and amplitude extraction from a single defocused image of a homogeneous object, J. Microsc. **206**, 33 (2002).
[9] T. E. Gureyev, Composite techniques for phase retrieval in the Fresnel region, Opt. Commun. **220**, 49 (2003).
[10] X. Wu and H. Liu, A general theoretical formalism for x-ray phase contrast imaging, J. X-Ray Sci. Technol. **11**, 33 (2003).
[11] X. Wu and H. Liu, A new theory of phase-contrast x-ray imaging based on Wigner distributions, Med. Phys. **31**, 2378 (2004).
[12] T. E. Gureyev, A. Pogany, D. M. Paganin, and S. W. Wilkins, Linear algorithms for phase retrieval in the Fresnel region, Opt. Commun. **231**, 53 (2004).
[13] X. Wu and H. Liu, Phase-space formulation for phase-contrast x-ray imaging, Appl. Opt. **44**, 5847 (2005).
[14] T. E. Gureyev, Ya. I. Nesterets, D. M. Paganin, A. Pogany, and S. W. Wilkins, Linear algorithms for phase retrieval in the Fresnel region. 2. Partially coherent illumination, Opt. Commun. **259**, 569 (2006).
[15] J. P. Guigay, M. Langer, R. Boistel, and P. Cloetens, Mixed transfer function and transport of intensity equation for phase retrieval in the Fresnel region, Opt. Lett. **32**, 1617 (2007).
[16] M. Langer, P. Cloetens, J.-P. Guigay, and F. Peyrin, Quantitative comparison of direct phase retrieval algorithms in in-line phase tomography, Med. Phys. **35**, 4556 (2008).
[17] L. De Caro, A. Cedola, C. Giannini, I. Bukreeva, and S. Lagomarsino, In-line phase-contrast imaging for strong absorbing objects, Phys. Med. Biol. **53**, 6619 (2008).
[18] F. Meng, H. Liu, and X. Wu, Feasibility study of the iterative x-ray phase retrieval algorithm, Appl. Opt. **48**, 91 (2009).
[19] F. Meng, D. Zhang, X. Wu, and H. Liu, A comparison of iterative algorithms and a mixed approach for in-line x-ray phase retrieval, Opt. Commun. **282**, 3392 (2009).
[20] D. X. Shi and M. A. Anastasio, Relationships between smooth- and small-phase conditions in x-ray phase-contrast imaging, IEEE Trans. Med. Imaging **28**, 1969 (2009).

[21] C. Y. Chou, Y. Huang, D. Shi, and M. A. Anastasio, Image reconstruction in quantitative x-ray phase-contrast imaging employing multiple measurements, Opt. Express **15**, 10002 (2007).
[22] D. M. Paganin, *Coherent X-Ray Optics* (Oxford University Press, New York, 2006).
[23] T. E. Gureyev, T. J. Davis, A. Pogany, S. C. Mayo, and S. W. Wilkins, Optical phase retrieval by use of first Born- and Rytov-type approximations, Appl. Opt. **43**, 2418 (2004).
[24] D. Paganin, A. Barty, P. J. McMahon, and K. A. Nugent, Quantitative phase-amplitude microscopy III: The effects of noise, J. Microsc. **214**, 51 (2004).
[25] A. Barty, K. A. Nugent, A. Roberts, and D. Paganin, Quantitative phase tomography, Opt. Commun. **175**, 329 (2000).
[26] M. P. Iturralde, *CRC Dictionary and Handbook of Nuclear Medicine and Clinical Imaging* (CRC Press, Boca Raton, FL, 1990).
[27] R. P. Yu, D. M. Paganin, and M. J. Morgan, Inferring nonlinear parabolic field equations from modulus data, Phys. Lett. A **341**, 156 (2005).
[28] D. Paganin and K. A. Nugent, Phase measurement of waves that obey non-linear equations, Opt. Lett. **27**, 622 (2002).
[29] J. A. Schmalz, T. E. Gureyev, D. M. Paganin, and K. M. Pavlov, Phase retrieval using radiation and matter-wave fields: Validity of Teague's method for solution of the transport-of-intensity equation, Phys. Rev. A **84**, 023808 (2011).
[30] E. Madelung, Quantentheorie in hydrodynamischer Form, Z. Phys. **40**, 322 (1926).
[31] T. E. Gureyev, A. Roberts, and K. A. Nugent, Phase retrieval with the transport of intensity equation: matrix solution with use of Zernike polynomials, J. Opt. Soc. Am. A **12**, 1932 (1995).
[32] T. E. Gureyev, S. Mayo, S. W. Wilkins, D. Paganin, and A. W. Stevenson, Quantitative In-Line Phase-Contrast Imaging with Multienergy X Rays, Phys. Rev. Lett. **86**, 5827 (2001).
[33] L. D. Turner, B. B. Dhal, J. P. Hayes, A. P. Mancuso, K. A. Nugent, D. Paterson, R. E. Scholten, C. Q. Tran, and A. G. Peele, X-ray phase imaging: Demonstration of extended conditions for homogeneous objects, Opt. Express **12**, 2960 (2004).
[34] X. Wu, H. Liu, and A. Yan, X-ray phase-attenuation duality and phase retrieval, Opt. Lett. **30**, 379 (2005).
[35] P. Cloetens (private communication).
[36] D. Paganin and K. A. Nugent, Noninterferometric Phase Imaging with Partially Coherent Light, Phys. Rev. Lett. **80**, 2586 (1998).
[37] T. W. Baillie, T. E. Gureyev, J. A. Schmalz, and K. M. Pavlov, Phase-contrast x-ray tomography using Teague's method, Opt. Express **20**, 16913 (2012).
[38] A. V. Bronnikov, Reconstruction formulas in phase-contrast tomography, Opt. Commun. **171**, 239 (1999).
[39] A. V. Bronnikov, Theory of quantitative phase-contrast computed tomography, J. Opt. Soc. Am. A **19**, 472 (2002).
[40] T. E. Gureyev, D. M. Paganin, G. R. Myers, Ya. I. Nesterets, and S. W. Wilkins, Phase-and-amplitude computer tomography, Appl. Phys. Lett. **89**, 034102 (2006).
[41] A. Groso, R. Abela, and M. Stampanoni, Implementation of a fast method for high resolution phase contrast tomography, Opt. Express **14**, 8103 (2006).
[42] S. Bajt, A. Barty, K. A. Nugent, M. McCartney, M. Wall, and D. Paganin, Quantitative phase-sensitive imaging in a transmission electron microscope, Ultramicroscopy **83**, 67 (2000).
[43] M. De Graef and Y. Zhu, Quantitative noninterferometric Lorentz microscopy, J. Appl. Phys. **89**, 7177 (2001).
[44] W. H. Press, S. A. Teukolsky, W. T. Vetterling, and B. P. Flannery, *Numerical Recipes in C, The Art of Scientific Computing*, 2nd ed. (Cambridge University Press, Cambridge, 1995).
[45] T. Gureyev, Ya. Nesterets, D. Thompson, S. Wilkins, A. Stevenson, A. Sakellariou, J. Taylor, and D. Ternovski, Toolbox for advanced x-ray image processing, Proc. SPIE **8141**, 81410B (2011).